connexins and green (EGFP) or red fluorescent protein (DsRED2), respectively. Site-directed mutagenesis was performed by QuikChange (Stratagene) as per manufacturer's instructions. Sequences of PCR-amplified regions were verified for both strands. For EGFP-tagged Cx40 plasmid, the1.1 kb coding sequence of WT and Q58L Cx40 were PCR-amplified by the following primers.

Forward (Cx40-F2X) 5'-AACAAGCTTCACCATGGGCGATTGGAGCTTCCT-3'

Reverse (Cx40-R5X) 5'-GCGGATCCACTGATAGGTCATCTGA-3'

(Underlines represent the restriction recognition sequences for HindIII and BamHI, respectively.) The PCR fragment was digested with HindIII/BamHI and subcloned in frame into the plasmid pEGFP-N1 (Takara Bio), generating fusion constructs (pEGFPN1-Cx40-WT and pEGFPN1-Cx40-Q58L). FLAG-tagged Cx40 plasmids were constructed by replacing the 0.8 kb EGFP fragment of the pEGFPN1-Cx40 plasmids in frame with the FLAG epitope (DYKDDDDK) cDNA at the C-terminal of the Cx40 (pCMV-FLAG-Cx40-WT and pCMV-FLAG-Cx40-Q58L, respectively. EGFP-tag or FLAG-tag did not change the conductance or the gating properties of Cx40 (data not shown).

Bicistronic constructs of WT-Cx40 and Q58L-Cx40 were made using the plasmid pIRES (Takara Bio). The WT-Cx40 (1.1 kb) and EGFP-tagged Q58L-Cx40 (1.8kb) were subcloned either at the upstream or the downstream cloning sites of the IRES (internal ribosomal entry site) (Fig 6B, constructs 3 and 4). Homomeric WT-Cx40 construct and the heteromeric constructs (WT-IRES-Q58L and Q58L-IRES-WT) in Fig 6C were constructed by PCR. WT-Cx40 or Q58L-Cx40 cDNAs were initially PCR-amplified by the primers Cx40-Fa and Cx40-Rb, and the PCR products were digested with NheI/EcoRI and subcloned in the upper multiple cloning sites NheI/EcoRI of pIRES.

Forward (Cx40-Fa) 5'-GCGCTAGCCACCATGGGCGATTGGAGC TTCCT-3'

Reverse (Cx40-Rb) 5'-AGAATTCTCACACTGATAGGTCATCTG-3'

(Underlines represent the restriction recognition sequences for NheI and EcoRI, respectively)

Similarly, WT-Cx40 or Q58L-Cx40 cDNAs were PCR-amplified by the primers Cx40-F8 and Cx40-R3, and the PCR products were digested with XbaI/NotI and subcloned in the lower multiple cloning sites XbaI/NotI of pIRES.

Forward (Cx40-F8) 5'-GCTCTAGACACCATGGGCGATTGGAGC TTCCT-3'

Reverse (Cx40-R3) 5'-ATAAGATGCGGCCGCTCACACTGATAGGTCATCTG-3'

(Underlines represent the restriction recognition sequences for XbaI and NotI, respectively)

Translation rate of the upstream cloned gene is generally greater than that cloned at the downstream site. Expression levels of WT-Cx40 (40 kDa) and Q58L-Cx40-GFP (67 kDa) are determined by western blotting using ant-Cx40 antibody.

3. Cell culture and transfection

Connexin 40 constructs were introduced into connexin-deficient HeLa cells or mouse neuroblastoma (N2A) cells, maintained in F-12 or Minimum Essential Medium, respectively, supplemented with 10% fetal bovine serum. HeLa and N2A cells were transfected with plasmids using Lipofectamine LTX or Lipofectamine 2000 (Invitrogen) as per the manufacturer's protocol.

4. Electrophysiology

Gap junction currents from heterologously expressed N2A cell pairs were recorded using whole-cell double patch clamp techniques as previously described.[9, 10] Recordings were carried out independently in each cell of a pair using two Axopatch 200B amplifiers (Axon Instruments). Current signals were filtered at 100-200 Hz and digitally sampled at 1-2 KHz

using an analog-to-digital interface (Digidata 1322A, Axon Instruments). The data were analyzed using Clampfit 9.2 (Axon Instruments) and Origin 7.5 (Origin Lab). The external solution contained (in mmol/L) 160 NaCl, 10 CsCl, 2 $CaCl_2$, 0.6 $MgCl_2$ and 10 HEPES, at pH 7.4. The intracellular (pipette) solution contained (in mmol/L) 130 $CsCl_2$, 0.5 $CaCl_2$, 10 HEPES, 10 EGTA, 2 Na_2ATP and 3 MgATP (added daily), (pH = 7.2). Pipette resistance was 5-10 MΩ. Octanol was added directly to the external solution at the final concentration of 1 mmol/L at each experiment. Experiments were carried out at room temperature (20-22 °C). All the chemicals were purchased from Sigma or Wako (Tokyo, Japan).

Gap junction channel conductance (g_j) was determined by conventional methods. Briefly, both cells in the pair ($cell_1$ and $cell_2$) were independently voltage-clamped at the same holding potential (-40 mV). $Cell_1$ was then stepped to a new voltage, thus creating a potential difference across the junction (V_j). The current in $cell_2$ was considered equal and opposite to the junctional current (I_j), and g_j was measured from the ratio I_j/V_j. The pulses were 2 or 5 sec in duration with an interpulse interval of 15 sec. Unitary conductance was obtained from pairs where only one or two functional channels were spontaneously detected. In some cases, cells were uncoupled by exposure to 1 mmol/L octanol. Histograms of events were obtained from channels recorded during repetitive 10-20 sec steps to V_j= +60 mV. To measure unitary conductance, only junctional current traces with events that lasted for longer than 20 ms were included. [9, 10] All-points histograms of digitized current traces and the frequency distribution histograms were constructed using Origin 7.5.

To analyze the electrophysiological properties of heterotypic gap junctions consisting of Cx40-WT and Cx40-Q58L, N2A cells were transiently transfected with either Cx40-WT (pIRES2-EGFP plasmid) or Cx40-Q58L (pIRES2-DsRED2 plasmid). Sixteen hours later, both cells were split with trypsin/EDTA and co-cultured. On the following day, the

heterotypic cell pairs of Cx40-WT (green) and Cx40-Q58L (red) were visually identified under fluorescent microscopy. Experiments were carried out at room temperature (20-22 ºC).

5. Immunocytochemistry

HeLa cells were cultured on a glass-bottom dish (Asahi Techno Glass, Chiba, Japan) and transfected with the fusion plasmids of pEGFPN1-Cx40-WT, pCMV-FLAG-Cx40-Q58L, or both. Next day, the cells were washed with phosphate-buffered saline (PBS), fixed in PBS containing 2% formaldehyde for 30 min at 4 °C, and permeabilized with 0.05% Triton X-100 for 30 min at 4 °C. After blocking with PBS containing 4% bovine serum albumin for 1 h at room temperature, the cells were stained with anti-FLAG M2 antibody (mouse monoclonal, 1:200, Sigma) for 1 h at room temperature. Protein reacting with antibody was visualized with Alexa 546-labeled secondary antibody (goat, 1:300, Invitrogen). EGFP and Alexa 546 fluorescence images were recorded with a FluoView FV1000 confocal microscope (Olympus Co, Tokyo) with a 60x oil immersion objective.

6. Western blotting

N2A cells maintained in a 6 well dish were transiently transfected with 3 μg Cx40 plasmids. Two days after transfection, cells were washed with PBS, and total cell lysate was extracted with lysis buffer including 50 mM Tris (pH7.5), 150 mM NaCl, 1% TritonX-100, 0.1 μg/ml aprotinin, 1x complete protease inhibitor (Roche Applied Science). Lysates precleared by centrifugation at 15,000 xg for 10 min were subjected to SDS-PAGE and immunoblotting with rabbit anti-Cx40 antibody (Millipore). Proteins reacting with primary antibodies were visualized by ECL system (GE Healthcare). The membrane was reprobed by anti-GAPDH antibody (Sigma).

7. Surface biotinylation

HeLa cells plated on 100 mm dishes were transiently transfected with 11 μg of pEGFPN1-Cx40-Q58L using Lipofectamine 2000 (Invitrogen). Surface biotinylation was performed 48 hours after transfection using the Pierce Cell Surface Protein Isolation Kit (Thermo Scientific, #89881) as per the manufacturer's protocol. Briefly, after 30 min of biotin labeling reaction at 4 °C, cell were lysed, mixed with NeutrAvidin agarose, and loaded on a column. The biotinylated proteins were eluted with the elution buffer. Fractions of the flowthrough, elute, and input lysate (1:1 diluted with lysate buffer) were subjected to a 4-12% gradient SDS-PAGE and immunobotting with anti-Cx40 antibodies (Cx40-A, 1:50 dilution, Alpha Diagnostic International). Proteins reacting with primary antibodies were visualized by LI-COR infrared imaging technology. Detection was done using anti-rabbit IRDye 800CW (1:10,000) antibodies (LI-COR Biosciences, # 926-32213).

8. Functional evaluation of novel *SCN5A* mutations associated with PFHB1

Three novel *SCN5A* mutations associated with PFHB1 were identified; a missense mutation F777L, a compound heterozygous frame shift mutation p.P701fsX710 plus p.P2006fsX2037, and a frame shift mutation pV1764fsX1786. These mutations were not found in 400 unaffected control alleles. Functional properties of these mutations were evaluated by whole-cell patch clamp. The mammalian expression plasmids encoding the mutations were constructed by site-directed mutagenesis as we described previously using a human Na channel α subunit (Nav1.5) cDNA.[11] The human cell line tsA-201 was transiently transfected together with Na channel β1 subunit, and the whole-cell Na currents were recorded as we previously described.[11] Electrode resistance ranged from 0.8 to 1.5 MΩ. Data

acquisition was carried out using an Axopatch 200B patch clamp amplifier and pCLAMP10 software (Axon Instruments). Currents were filtered at 5 kHz (–3 dB; 4-pole Bessel filter) and digitized using an analog-to-digital interface (Digidata 1440A; Axon Instruments). Experiments were carried out at room temperature (20–22°C). Voltage errors were minimized using series resistance compensation (generally 80%). Cancellation of the capacitance transients and leak subtraction were performed using an online P/4 protocol. The pulse protocol cycle time was 10 s. The data were analyzed using Clampfit 10 (Axon Instruments) and SigmaPlot 11 (SPSS Science). The holding potential was –120 mV. The bath solution contained (in mmol/l): 145 NaCl, 4 KCl, 1.8 $CaCl_2$, 1 $MgCl_2$, 10 HEPES, and 10 glucose, pH 7.35 (adjusted with NaOH). The pipette solution (intracellular solution) contained (in mmol/l): 10 NaF, 110 CsF, 20 CsCl, 10 EGTA, and 10 HEPES, pH 7.35 (adjusted with CsOH). The time from establishing the whole-cell configuration to onset of recording was consistent cell-to-cell to exclude the possible time-dependent shift of steady-state inactivation. To determine activation parameters, the current-voltage relationship was fit to the Boltzmann equation $I = (V - V_{rev}) \times G_{max} \times (1 + \exp[V - V_{1/2}] / k)^{-1}$, where I is the peak Na current during the test pulse potential V. The parameters estimated by the fitting are V_{rev} (reversal potential), G_{max} (maximum conductance), and k (slope factor) (Supplemental Figure 1B). Steady-state availability for fast inactivation was measured with a standard double-pulse protocol (Supplemental Figure 1C, left inset), and the data were fit with the Boltzmann equation $I/I\text{max} = (1 + \exp[(V - V_{1/2}) / k])^{-1}$, where I_{max} is the maximum peak Na current, to determine the membrane potential for $V_{1/2}$ and k. Functional properties of other mutations in *SCN5A* or *SCN1B* were previous reported (Supplemental table S1).

SUPPLEMENTAL FIGURE LEGEND

Supplemental Figure S1

Functional properties of the novel *SCN5A* mutations

Panel A shows whole-cell Na currents recorded from tsA201cells expressing wild type (WT) Nav1.5 (left) or Nav1.5 mutant F777L (right). Currents were elicited by step pulses from -90 mV to +60 mV (10 mV step) from a holding potential of -120 mV. Bars: 5 msec and 2 nA. Non-inactivated late currents were not observed. Panel B shows current-voltage relationship. Average peak current density was significantly reduced in F777L ($p<0.001$). WT: 391.7±47.1 pA/pF, n=15 (open circles). F777L: 301.2±30.0 pA/pF, n=9 (closed circles). Panel C shows that the voltage-dependence of activation of F777L channels (closed circles) was not different from control, whereas steady-state inactivation curve was significantly shifted in the hyperpolarizing direction in F777L (WT: $V_{1/2}$= -87.1±0.5 mV, n=25; F777L: $V_{1/2}$= -92.4 ± 1.3 mV, n=9; $p<0.001$). These biophysical properties suggest a decrease in the number of functional (conductive) sodium channels during the action potential upstroke consequent to the mutation. Previous studies have revealed that mutations A1180V[12] and D1275N[13], also found in our series (see supplemental Table S1), exhibit minor functional abnormalities when expressed in cultured cells, though more drastic changes are observed when the channels are expressed in cardiomyocytes[14]. Cells expressing compound heterozygous mutations p.P701fsX710 and p.P2006fsX2037, or a frame shift mutation pV1764fsX1786, exhibited no Na current, suggesting haploinsufficiency of cardiac Na current in the afflicted population.

Supplemental Figure S2

Exercise stress test of the proband's mother

Electrocardiographic recording obtained from the probands's mother during a treadmill exercise stress test at the age of 16. A heart rate of 177 bpm was achieved after 9 min 20 sec of exercise test by Bruce protocol. During the recovery phase at 1 min 17 sec, superior axis narrow QRS ventricular tachycardia with a rate of 110 bpm was observed (upper panel) .Ventricular tachycardia was spontaneously terminated at 20 min 23 sec of the recovery phase (lower panel).

Supplemental Figure S3

Co-expression of Cx40-WT and Cx40-Q58L in N2A cells.

Panels A-C show fluorescence images from a cell pair recorded from cells co-transfected with pIRES2-EGFP-Cx40-WT and pIRES2-DsRED2-Cx40-Q58L (0.5 μg each). Notice expression of both the green (A) and the red marker (B), giving a yellow color in the overlay (C). Calibration bar: 20 μm. Panel D: Junctional conductance recorded from cell pairs as that shown in panels A-C was 18.9±5.4 nS (n=6). This number was not statistically different from that obtained from pairs expressing WT-GFP and Q58L-GFP (average Gj= 13.0±2.4 nS; n=17).

Supplemental Figure S4

Surface biotinylation of Q58L-Cx40 expressed in HeLa cells.

HeLa cells transfected with pEGFPN1-Cx40-Q58L were surface-labeled with biotin, and lysed. Cell lysate was mixed with NeutrAvidin agarose and loaded on a column. Flowthough, elute (biotin-labeled membrane fraction) and the input lysate (1:1 diluted with lysate buffer) were subjected to SDS-PAGE and immunoblotting. A single 67KDa band of similar intensity

was detected in both elute and the input lysate, but not in the flowthrough. These data indicate that mutation Q58L did not prevent surface expression of the Cx40 protein.

SUPPLEMENTAL REFERENCES

1. Wang Q, Li Z, Shen J, Keating MT. Genomic organization of the human SCN5A gene encoding the cardiac sodium channel. *Genomics*. 1996;34:9-16
2. Splawski I, Shen J, Timothy KW, Lehmann MH, Priori S, Robinson JL, Moss AJ, Schwartz PJ, Towbin JA, Vincent GM, Keating MT. Spectrum of mutations in long-QT syndrome genes. KVLQT1, HERG, SCN5A, KCNE1, and KCNE2. *Circulation*. 2000;102:1178-1185
3. Plaster NM, Tawil R, Tristani-Firouzi M, Canun S, Bendahhou S, Tsunoda A, Donaldson MR, Iannaccone ST, Brunt E, Barohn R, Clark J, Deymeer F, George AL, Jr., Fish FA, Hahn A, Nitu A, Ozdemir C, Serdaroglu P, Subramony SH, Wolfe G, Fu YH, Ptacek LJ. Mutations in Kir2.1 cause the developmental and episodic electrical phenotypes of Andersen's syndrome. *Cell*. 2001;105:511-519.
4. Makita N, Sloan-Brown K, Weghuis DO, Ropers HH, George AL, Jr. Genomic organization and chromosomal assignment of the human voltage-gated Na^+ channel beta 1 subunit gene (SCN1B). *Genomics*. 1994;23:628-634
5. Watanabe H, Koopmann TT, Le Scouarnec S, Yang T, Ingram CR, Schott JJ, Demolombe S, Probst V, Anselme F, Escande D, Wiesfeld AC, Pfeufer A, Kaab S, Wichmann HE, Hasdemir C, Aizawa Y, Wilde AA, Roden DM, Bezzina CR. Sodium channel beta1 subunit mutations associated with Brugada syndrome and cardiac conduction disease in humans. *J. Clin. Invest.* 2008;118:2260-2268
6. Medeiros-Domingo A, Kaku T, Tester DJ, Iturralde-Torres P, Itty A, Ye B, Valdivia C, Ueda K, Canizales-Quinteros S, Tusie-Luna MT, Makielski JC, Ackerman MJ. *SCN4B*-encoded sodium channel β4 subunit in congenital long-QT syndrome. *Circulation*. 2007;116:134-142

7. Schulze-Bahr E, Neu A, Friederich P, Kaupp UB, Breithardt G, Pongs O, Isbrandt D. Pacemaker channel dysfunction in a patient with sinus node disease. *J. Clin. Invest.* 2003;111:1537-1545

8. Britz-Cunningham SH, Shah MM, Zuppan CW, Fletcher WH. Mutations of the connexin43 gap-junction gene in patients with heart malformations and defects of laterality. *New Engl. J. Med.* 1995;332:1323-1330

9. Seki A, Coombs W, Taffet SM, Delmar M. Loss of electrical communication, but not plaque formation, after mutations in the cytoplasmic loop of connexin43. *Heart Rhythm.* 2004;1:227-233

10. Anumonwo JMB, Taffet SM, Gu H, Chanson M, Moreno AP, Delmar M. The carboxyl terminal domain regulates the unitary conductance and voltage dependence of connexin40 gap junction channels. *Circ. Res.* 2001;88:666-673

11. Makita N, Behr E, Shimizu W, Horie M, Sunami A, Crotti L, Schulze-Bahr E, Fukuhara S, Mochizuki N, Makiyama T, Itoh H, Christiansen M, McKeown P, Miyamoto K, Kamakura S, Tsutsui H, Schwartz PJ, George AL, Roden DM. The E1784K mutation in SCN5A is associated with mixed clinical phenotype of type 3 long QT syndrome. *J. Clin. Invest.* 2008;118:2219-2229

12. Ge J, Sun A, Paajanen V, Wang S, Su C, Yang Z, Li Y, Wang S, Jia J, Wang K, Zou Y, Gao L, Wang K, Fan Z. Molecular and clinical characterization of a novel SCN5A mutation associated with atrioventricular block and dilated cardiomyopathy. *Circ Arrhythmia Electrophysiol.* 2008;1:83-92

13. Groenewegen WA, Firouzi M, Bezzina CR, Vliex S, van Langen IM, Sandkuijl L, Smits JP, Hulsbeek M, Rook MB, Jongsma HJ, Wilde AA. A cardiac sodium channel mutation cosegregates with a rare connexin40 genotype in familial atrial standstill.

Circ. Res. 2003;92:14-22

14. Watanabe H, Nogami A, Ohkubo K, Kawata H, Hayashi Y, Ishikawa T, Makiyama T, Nagao S, Yagihara N, Takehara N, Kawamura Y, Sato A, Okamura K, Hosaka Y, Sato M, Fukae S, Chinushi M, Oda H, Okabe M, Kimura A, Maemura K, Watanabe I, Kamakura S, Horie M, Aizawa Y, Shimizu W, Makita N. Electrocardiographic Characteristics and SCN5A Mutations in Idiopathic Ventricular Fibrillation Associated with Early Repolarization. *Circulation: Arrhythmia and Electrophysiology*. 2011

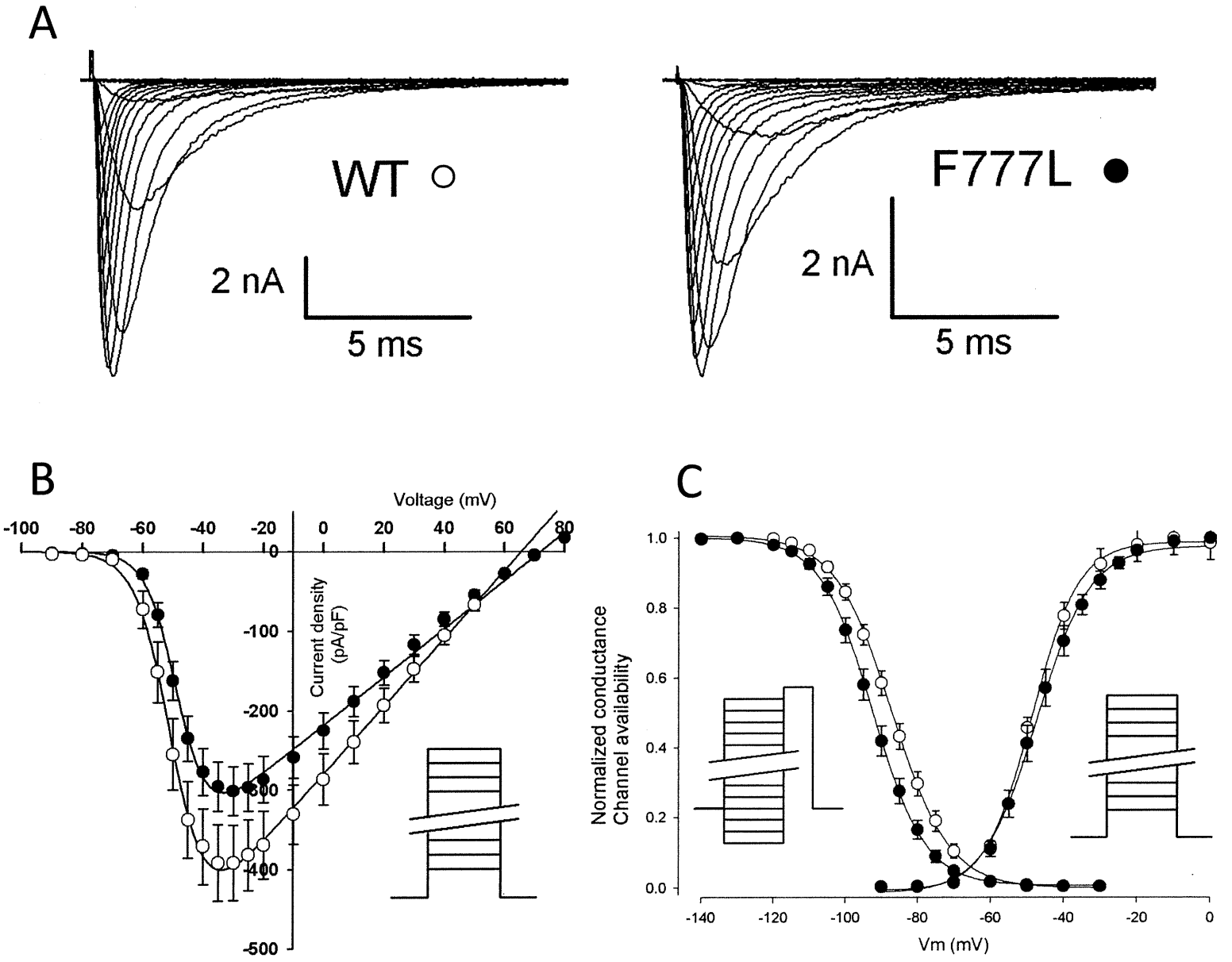

VT initiation at 1'17" (recovery phase)

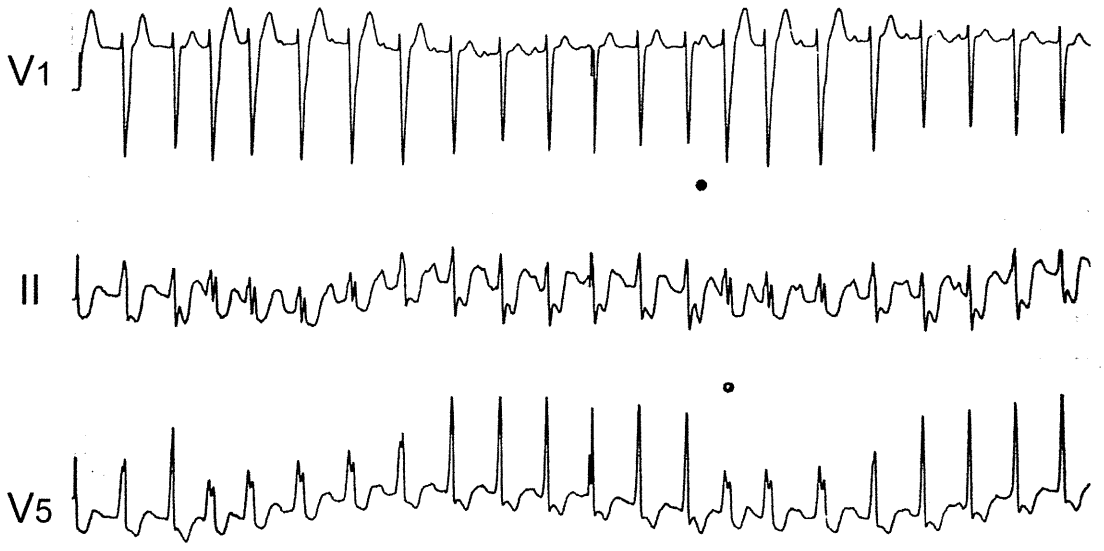

Spontaneous VT termination at 20'23"

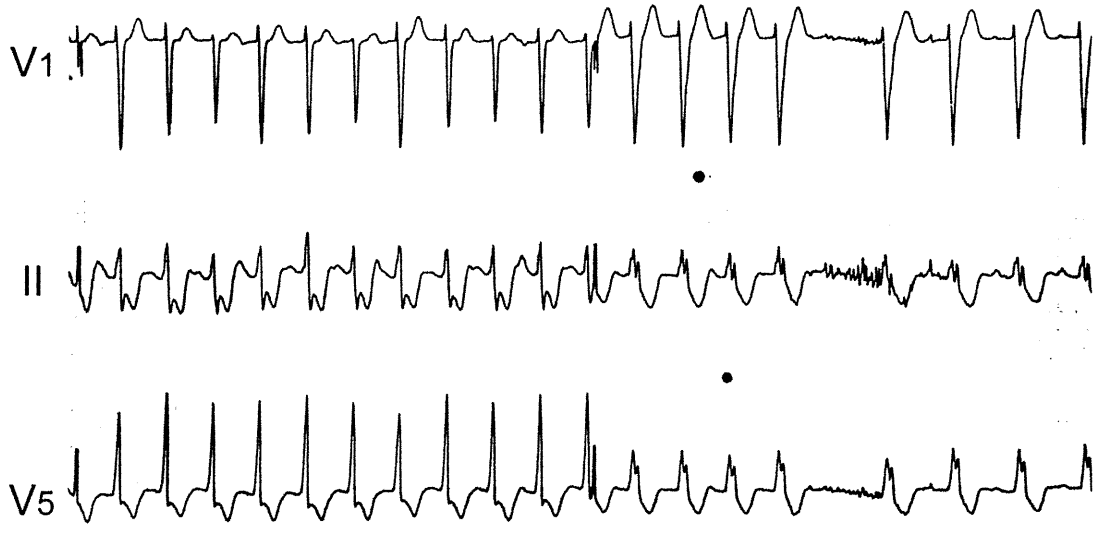

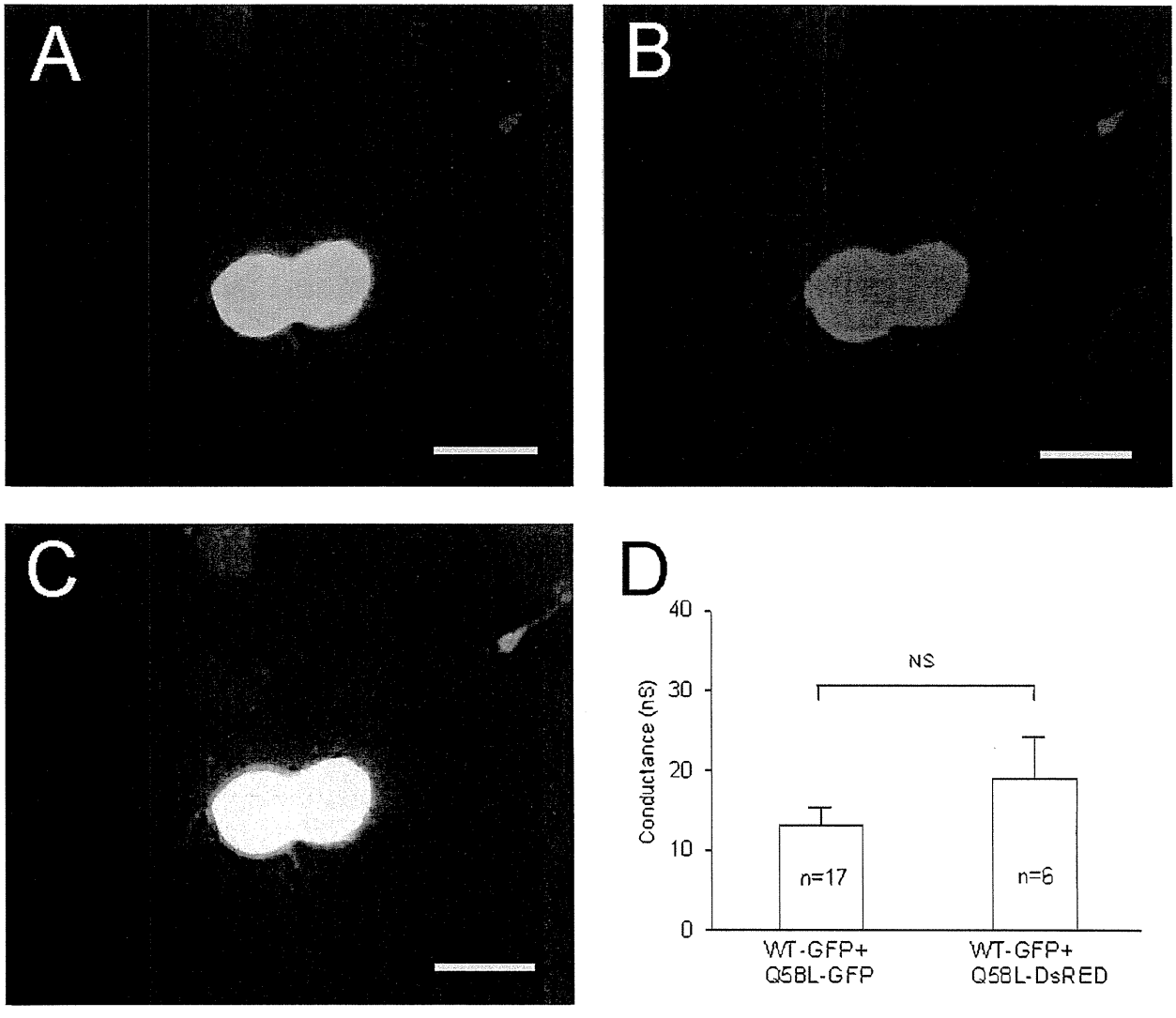

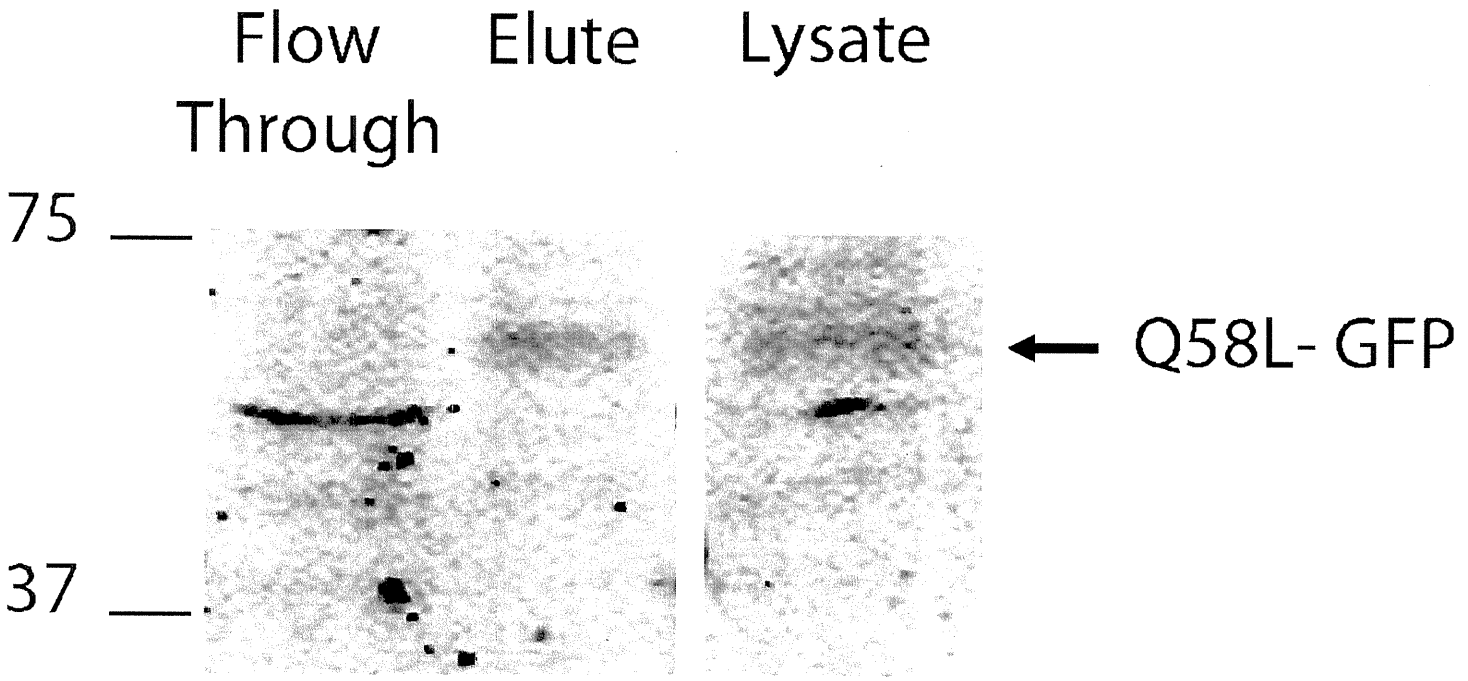

Supplemental Table S1. Genetic mutations identified in PFHBI probands

Patient	Gene	Exon	cDNA mutation	Amino acid change	Mutation type	Phenotype	Reference
1 †	*GJA5*	2	c.173 A>T	Q58L	Missense	PFHBI	this study
2	*SCN5A*	15	c.2329T>C	F777L	Missense	PFHBI +DCM+MMD	this study
3 †*	*SCN5A*	14	c.2102 del C	p.P701fsX710	Deletion	PFHBI +BrS	this study
	SCN5A	28	c.6017 delC	p.P2006fsX2037	Deletion		this study
4	*SCN5A*	28	c.5290 delG	p.V1764fsX1786	Deletion	PFHBI +BrS+MMD	this study
5	*SCN5A*	20	c.3539C>T	A1180V	Missense	PFHBI +DCM	[11]
6	*SCN5A*	21	c. 3823G>A	D1275N	Missense	PFHBI +DCM	[12]
7	*SCN5A*	Int22	IVS22+2T>C		Exon skipping	PFHBI	[13]
8	*SCN5A*	28	c.5280 delG	p.A1711fsX1786	Deletion	PFHBI	[13]
9	*SCN5A*	28	c. 5129C>T	S1710L	Missense	PFHBI +IVF	[14]
10	*SCN1B*	3	c.259G>C	E87Q	Missense	PFHBI	[5]
11	*SCN1B*	3A	c.536G>A	W179X	Missense	PFHBI+BrS	[5]
12	*SCN1B*	3A	c.537G>A	W179X	Missense	PFHBI	[5]

GJA5: connexin 40, *SCN5A*: cardiac voltage-gated Na channel α subunit, *SCN1B*: voltage-gated Na channel β1 subunit

†: Patients 1 and 3 are sudden cardiac death victims

*: Patient 3 is a compound heterozygous carrier of *SCN5A* mutations

DCM: dilated cardiomyopathy, MMD: myotonic muscular dystrophy, BrS: Brugada syndrome, IVF: idiopathic ventricular fibrillation, Int22: Intron 22

Supplemental Table S2. ECG parameters of the family members

Family	Age	HR (bpm)	PR (ms)	QRS (ms)	QTc (ms)	Axis (degree)	ST depression
Proband	6	87	*	126	421	-8	II,III,aVF, V3-6
	8	77	*	128	396	-21	II,III,aVF, V2-6
Sister	6	86	130	86	404	-25	II,III,aVF, V3-6
	11	85	142	88	416	-49	II,III,aVF, V3-6
Mother	16	63	248	152	471	-25	II,III,aVF, V3-6

*: advanced AV block

Regional cooling facilitates termination of spiral-wave reentry through unpinning of rotors in rabbit hearts

Masatoshi Yamazaki, MD, PhD,*† Haruo Honjo, MD, PhD,* Takashi Ashihara, MD, PhD,‡ Masahide Harada, MD, PhD,* Ichiro Sakuma, PhD,§ Kazuo Nakazawa, PhD,‖ Natalia Trayanova, PhD, FHRS, FAHA,¶ Minoru Horie, MD, PhD,‡ Jérôme Kalifa, MD, PhD,† José Jalife, MD, FHRS,† Kaichiro Kamiya, MD, PhD,* Itsuo Kodama, MD, PhD*

*From the *Department of Cardiovascular Research, Research Institute of Environmental Medicine, Nagoya University, Nagoya, Japan, †Center for Arrhythmia Research, University of Michigan, Ann Arbor, Michigan, ‡Department of Cardiovascular and Respiratory Medicine, Shiga University of Medical Science, Otsu, Japan, §Graduate School of Engineering, The University of Tokyo, Tokyo, Japan, ‖National Cardiovascular Center, Research Institute, Suita, Japan, ¶Institute for Computational Medicine, Johns Hopkins University, Baltimore, Maryland.*

BACKGROUND Moderate global cooling of myocardial tissue was shown to destabilize 2-dimensional (2-D) reentry and facilitate its termination.

OBJECTIVE This study sought to test the hypothesis that regional cooling destabilizes rotors and facilitates termination of spontaneous and DC shock-induced subepicardial reentry in isolated, endocardially ablated rabbit hearts.

METHODS Fluorescent action potential signals were recorded from 2-D subepicardial ventricular myocardium of Langendorff-perfused rabbit hearts. Regional cooling (by 5.9°C ± 1.3°C) was applied to the left ventricular anterior wall using a transparent cooling device (10 mm in diameter).

RESULTS Regional cooling during constant stimulation (2.5 Hz) prolonged the action potential duration (by 36% ± 9%) and slightly reduced conduction velocity (by 4% ± 4%) in the cooled region. Ventricular tachycardias (VTs) induced during regional cooling terminated earlier than those without cooling (control): VTs lasting >30 seconds were reduced from 17 of 39 to 1 of 61. When regional cooling was applied during sustained VTs (>120 seconds), 16 of 33 (48%) sustained VTs self-terminated in 12.5 ± 5.1 seconds. VT termination was the result of rotor destabilization, which was characterized by unpinning, drift toward the periphery of the cooled region, and subsequent collision with boundaries. The DC shock intensity required for cardioversion of the sustained VTs decreased significantly by regional cooling (22.8 ± 4.1 V, n = 16, vs 40.5 ± 17.6 V, n = 21). The major mode of reentry termination by DC shocks was phase resetting in the absence of cooling, whereas it was unpinning in the presence of cooling.

CONCLUSION Regional cooling facilitates termination of 2-D reentry through unpinning of rotors.

KEYWORDS Spiral-wave reentry; Regional myocardial cooling; Unpinning; Optical mapping; Ventricular tachyarrhythmia

ABBREVIATIONS **2-D** = two-dimension; **3-D** = three-dimension; **APD** = action potential duration; **BCL** = basic cycle length; **BDM** = 2,3-butandione monoxime; **CV** = conduction velocity; **FBL** = functional block line; **ICD** = implantable cardioverter-defibrillator; **LV** = left ventricle; **PS** = phase singularity; **RC** = regional cooling; **SW** = spiral wave; **VF** = ventricular fibrillation; **VT** = ventricular tachycardia

(Heart Rhythm 2012;9:107–114)

Introduction

High-energy DC shock application by implantable cardioverter-defibrillator (ICD) is the most effective procedure for preventing sudden cardiac death resulting from ventricular tachycardia/ventricular fibrillation (VT/VF). Large-scale clinical trials have demonstrated that ICD therapy is superior over any pharmacological therapy to prevent cardiac death.[1,2] The usefulness of ICD therapy currently available is, however, limited by a number of adverse effects of high-energy shocks, such as myocardial damages causing arrhythmias, increased pacing threshold,[3,4] and mechanical dysfunction giving rise to hemodynamic deterioration.[5] In addition, painful DC shocks by ICD often cause serious psychological disorders.[6,7] Theoretical and experimental studies have revealed that spiral-wave (SW) reentry rotating around a functional obstacle is the major mechanism of VT/VF.[8,9] Arguably, should SW reentry be regulatable by procedures other than DC shocks or those combined with low-energy shocks, it could lead to innovative therapeutic

This study was supported by Grant-in-Aid for Scientific Research (B) 19390210 and (C) 20590860 from the Japanese Society for Promotion of Sciences and Grant-in-Aid for Scientific Research on Innovative Area 22136010 from the Ministry of Education, Culture, Sports, Science and Technology, Japan. **Address reprint requests and correspondence:** Dr. Haruo Honjo, Department of Cardiovascular Research, Research Institute of Environmental Medicine, Nagoya University, Furo-cho, Chikusa-ku, Nagoya 464-8601, Japan. E-mail address: honjo@riem.nagoya-u.ac.jp.

1547-5271/$ -see front matter doi:10.1016/j.hrthm.2011.08.013

modalities for prevention of arrhythmic death. Although several conceptual approaches have been proposed to terminate SW reentry by low-energy DC application, e.g., resonant drift,[10,11] controlling chaos,[12] synchronized pacing,[13,14] and unpinning of SWs,[15,16] feasibility of these approaches has not yet been validated. In isolated rabbit hearts, we have previously shown that moderate hypothermia facilitates termination of VT through destabilization (unpinning) of SW reentry.[17] Using high-density electrode mapping in rabbit hearts, Boersma et al[18] demonstrated that regional cooling (RC) of the ventricle during programmed electrical stimulation prevented stabilization of functional reentry and resulted in only brief episodes of polymorphic VT that terminated spontaneously. Here we hypothesized that moderate RC of the ventricular myocardium could be a novel procedure to destabilize already-established and sustained VT and lead to its termination. To test this hypothesis, we carried out high-resolution optical mapping experiments in 2-dimensional (2-D) ventricular myocardium.

Methods

Experimental model and optical mapping

The protocol was approved by the Institutional Animal Care and Use Committee at Nagoya University. The experimental model and procedures of optical mapping are essentially the same as reported previously.[17,19,20] Briefly, optical membrane potential signals were recorded from a 2-D ventricular muscle layer of Langendorff-perfused rabbit hearts subjected to endocardial cryoablation; 2,3-butandione monoxime (BDM) was applied to minimize motion artifacts. Action potential duration (APD) and conduction velocity (CV) were measured during constant pacing (basic cycle length [BCL] 180 to 400 ms) from the apex. The details of experimental procedures and data analysis are described in the Online Supplemental Methods.

RC

The temperature of the central region of the left ventricular (LV) free wall was temporarily reduced by applying a transparent cooling device (diameter, 10 mm) perfused with cold water and in abutting contact with the epicardial surface (Figure 1A). In pilot experiments using thermography (TVS-200, Nippon Avionics, Tokyo, Japan) (Figure 1B), we confirmed that the temperature in the target area was decreased by 5.9°C ± 1.3°C (n = 7, $P < .05$) from baseline (36.0°C). The temperature change was reversed completely after removal of the device. Temperature outside the cooled region remained unchanged.

Experimental protocols

Reentrant VTs (lasting ≥3 beats) were induced by modified cross-field stimulation using 1 of 2 protocols. First, in 8 hearts, VTs were induced before and 20 seconds after application of RC to compare their duration and dynamics. Second, in 15 additional hearts, sustained VTs (>120 seconds) were induced and RC was applied to observe its effects on VT duration and dynamics. If the sustained VTs did not terminate during the 30-second observation period of RC, 10-ms monophasic DC shocks were applied at in-

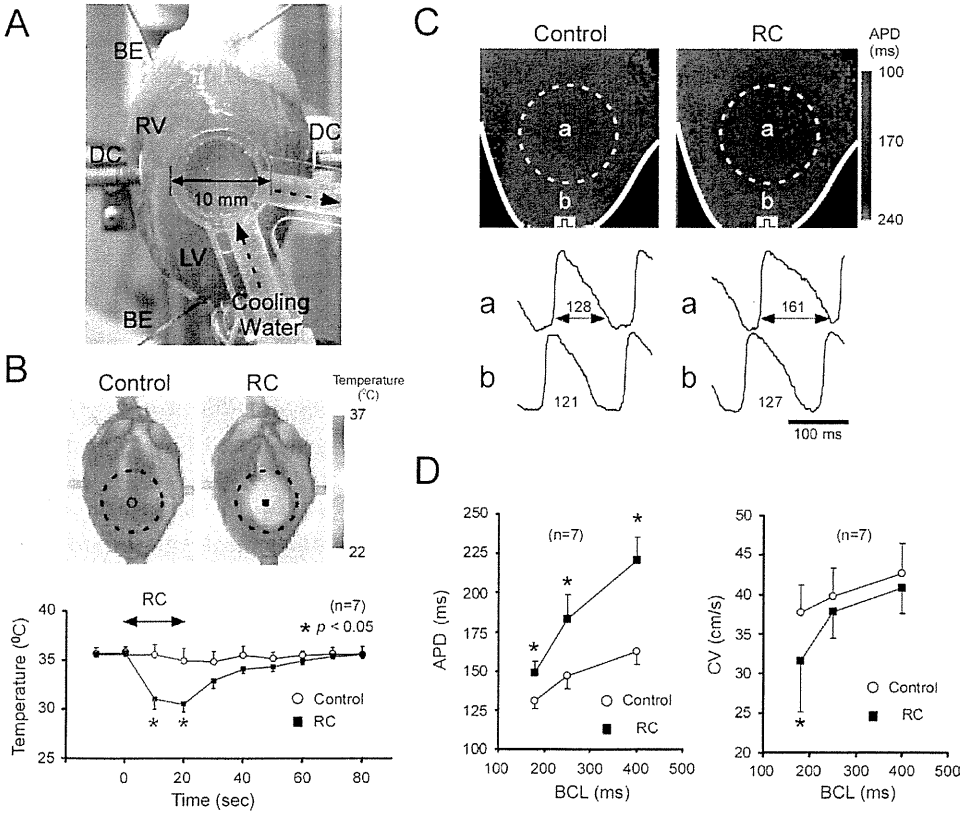

Figure 1 RC of 2-D rabbit hearts. **A:** A transparent cooling device (diameter, 10 mm) was in contact with the LV subepicardial surface, and water (20°C) was circulated inside the device. **B:** Thermography images (top) and changes of temperature (bottom) in response to RC. Those without RC served as control. *$P < .05$ vs control. **C:** Changes of APD (BCL, 400 ms) in response to RC. Top, APD color gradient maps with and without RC (control); bottom, optical action potential signals inside (a) and outside (b) the RC region. Numerals are APD (in ms). **D:** Effects of RC on APD (left) and CV (right) in the RC region at BCLs 180 to 400 ms. *$P < .05$ vs control (without RC). 2-D = two-dimension; APD = action potential duration; BCL = basic cycle length; BE = electrodes for recording distant bipolar electrograms; CV = conduction velocity; DC = paddle electrodes for DC-application; LV = left ventricle; RC = regional cooling.